Available online at www.sciencedirect.com
ScienceDirect
Remote Sensing of Environment xx (2007) xxx – xxx
Remote Sensing of Environment
www.elsevier.com/locate/rse

Impacts of spectral band difference effects on radiometric cross-calibration between satellite sensors in the solar-reflective spectral domain

P.M. Teillet [a,*], G. Fedosejevs [b], K.J Thome [c], John L. Barker [d]

[a] Department of Physics, University of Lethbridge, 4401 University Drive W., Lethbridge, Alberta, Canada T1K 3M4
[b] Canada Centre for Remote Sensing, 588 Booth Street, Ottawa, Ontario, Canada K1A 0Y7
[c] Remote Sensing Group, Optical Sciences Center, University of Arizona, 1630 E. University Blvd, Tucson, AZ 85721-0094, USA
[d] NASA's Goddard Space Flight Center, Code 614.4, Greenbelt, MD 20771, USA

Received 5 January 2007; received in revised form 19 March 2007; accepted 20 March 2007

Abstract

In order for quantitative applications to make full use of the ever-increasing number of Earth observation satellite systems, data from the various imaging sensors involved must be on a consistent radiometric scale. This paper reports on an investigation of radiometric calibration errors due to differences in spectral response functions between satellite sensors when attempting cross-calibration based on near-simultaneous imaging of common ground targets in analogous spectral bands, a commonly used post-launch calibration methodology. Twenty Earth observation imaging sensors (including coarser and higher spatial resolution sensors) were considered, using the Landsat solar reflective spectral domain as a framework. Scene content was simulated using spectra for four ground target types (Railroad Valley Playa, snow, sand and rangeland), together with various combinations of atmospheric states and illumination geometries. Results were obtained as a function of ground target type, satellite sensor comparison, spectral region, and scene content. Overall, if spectral band difference effects (SBDEs) are not taken into account, the Railroad Valley Playa site is a "good" ground target for cross calibration between most but not all satellite sensors in most but not all spectral regions investigated. "Good" is defined as SBDEs within ±3%. The other three ground target types considered (snow, sand and rangeland) proved to be more sensitive to uncorrected SBDEs than the RVPN site overall. The spectral characteristics of the scene content (solar irradiance, surface reflectance and atmosphere) are examined in detail to clarify why spectral difference effects arise and why they can be significant when comparing different imaging sensor systems. Atmospheric gas absorption features are identified as being the main source of spectral variability in most spectral regions. The paper concludes with recommendations on spectral data and tools that would facilitate cross-calibration between multiple satellite sensors.
© 2007 Elsevier Inc. All rights reserved.

Keywords: Radio calibration; Sensor cross-calibration; Spectral bands

1. Introduction

In order for quantitative Earth observation applications to make full use of the ever-increasing number of Earth observation satellite systems, data from the various imaging sensor systems must be on a consistent radiometric calibration scale (Slater et al., 2001) and hence sensor radiometric calibration is of critical importance. The methods and measurements involved in sensor radiometric calibration can be grouped into three domains (Dinguirard & Slater, 1999): on the ground prior to launch, onboard the spacecraft post-launch (including reference to lamp sources and/or solar illumination (e.g., Markham et al., 1997) or lunar illumination (Barnes et al., 1999; Godden & McKay, 1997; Kieffer & Wildey, 1996)), and approaches using Earth scenes imaged in-flight. This paper concerns the third domain: sensor radiometric calibration based on Earth scenes imaged in-flight.

Earth surfaces with suitable characteristics have long been used as benchmark or test sites to verify the post-launch radiometric calibration performance of satellite sensors. The associated methodologies are often referred to as vicarious or

* Corresponding author.
E-mail address: p.teillet@uleth.ca (P.M. Teillet).

0034-4257/$ - see front matter © 2007 Elsevier Inc. All rights reserved.
doi:10.1016/j.rse.2007.03.003

Table 1
Some of the published works on the use of terrestrial targets for the vicarious or ground-look calibration of satellite sensors are cited

Earth Target Type	Reference
Dry lake beds or playas	(Biggar et al., 2003; Gu et al., 1992; Rondeaux et al., 1998; Santer et al., 1992; Slater et al., 1987; Teillet et al., 1990; Thome, 2001; Thome et al., 1997, 1998, 2003a,b; Wheeler et al., 1994; Wu et al., 1997)
Deserts	(Cabot et al., 1999, 2000; Cosnefroy et al., 1996; Rao & Chen, 1995, 1999; Rao et al., 2003)
Ice or snow fields	(Loeb, 1997; Nieke et al., 2003; Six et al., 2004; Tahnk & Coakley, 2001)
Atmospheric scattering	(Iwabuchi, 2003; Kaufman & Holben, 1993; Martiny et al., 2005; Santer & Martiny, 2003)
Uniform cloud cover	(Iwabuchi, 2003; Kaufman & Holben, 1993; Vermote & Kaufman, 1998)
Ocean glint	(Kaufman & Holben, 1993; Vermote & Kaufman, 1998)
Semi-arid rangeland	(Teillet et al., 1998, 1999)
Grassland targets	(Black et al., 2003; Schiller, 2003)
Multiple target types	(Hill & Aifadopoulou, 1990; Koepke, 1982; Teillet et al., 1997a, 2001a,b)

The list does not include examples of the many articles that describe the use of pseudo-invariant features to normalize satellite imagery for multi-temporal analysis without yielding absolute radiometric calibration coefficients.

ground-look calibration. Table 1 lists some of the published work on the use of such methodologies. Many of these approaches use surface and atmospheric measurements to estimate top-of-atmosphere radiance at the entrance aperture of a given satellite sensor. This provides a check on, or an update of, the nominal sensor calibration and helps to monitor sensor performance over time. Historically, field measurement campaigns at calibration test sites typically targeted only one sensor per field sortie, but many of the more recent campaigns have concerned multiple sensors that passed over a given test site within a short time or on the same day (e.g., Thome et al., 2003a). Nevertheless, efforts such as these remain resource intensive and, therefore, it has also been of considerable interest to develop less expensive complementary approaches that can provide more frequent calibration updates, even if they are less accurate. In particular, the use of terrestrial targets to check on the radiometric calibration of a given satellite sensor without coincident surface measurements or to transfer radiometric calibration between satellite sensors (so-called cross-calibration) without coincident surface measurements has been on the increase. The possibility of taking advantage of autonomous in-situ sensors in this context is also being explored (Teillet et al., 2001a).

Central to vicarious calibration techniques is the level of radiometric accuracy that can be achieved. Error budgets have been reported (e.g., Biggar et al., 1994) but, with few exceptions (e.g., O'Brien & Mitchell, 2001), they have not yet been adapted to cross-calibration cases in the absence of ground-based measurements. Similarly, the question arises as to what uncertainties can be expected in applications that use derived quantities such as vegetation indices when utilizing results obtained from multiple imaging sensors.

This paper reports on an investigation of radiometric cross-calibration errors due to differences in spectral response functions between many of the satellite sensors used by the remote sensing community in the context of near-simultaneous imaging of common ground targets in analogous spectral bands. In particular, the simulation study assesses the impact of spectral band difference effects on cross-calibration if they are not or cannot be taken into account. Adequate consideration of spectral band differences may not be possible in the absence of ground-based spectral measurements or it may be approximate if historical spectra are used that are not necessarily representative of the test site on specific satellite-imaging days. The consideration of spectral band difference effects is becoming very important as more sensors are being used for quantitative analyses that require well-calibrated data. Different applications and technology developments in Earth observation necessarily require different spectral coverage. Thus, spectral bands differ significantly between sensors, even for bands designed to look at the same region of the electromagnetic spectrum, with the result that they yield fundamentally different measurements that are not directly comparable.

Given that the Landsat-7 Enhanced Thematic Mapper Plus (ETM+) is well-understood radiometrically (Markham et al., 2004), a consideration of spectral band effects on cross-calibration between the ETM+ and other imaging sensors was the starting point for the study. With comparisons between ETM+ and the other sensors in hand, it was straightforward to examine

Table 2
The twenty satellite sensor systems included in this study

(1) Landsat-7 Enhanced Thematic Mapper Plus (L7 ETM+)
(2) Landsat-5 Thematic Mapper (L5 TM)
(3) Landsat-4 Thematic Mapper (L4 TM)
(4) Advanced Earth Observing Satellite-1 (ADEOS-1) Advanced Visible and Near-Infrared Radiometer (AVNIR)
(5) Earth Observing-1 (EO-1) Advanced Land Imager (ALI)
(6) Terra Advanced Spaceborne Thermal Emission and Reflection (ASTER)
(7) Système Pour l'Observation de la Terre-5 (SPOT-5) High Resolution Geometric (HRG)
(8) Indian Remote Sensing satellite IRS P6 Resourcesat-1 Linear Imaging Self Scanner (LISS-III)
(9) Indian Remote Sensing satellite IRS-P6 Resourcesat-1 Advanced Wide Field Sensor (AWiFS)
(10) China–Brazil Earth Resources Satellite-2 (CBERS-2) High-Resolution CCD Camera (HRCC)
(11) China–Brazil Earth Resources Satellite-2 (CBERS-2) Infrared Multispectral Scanner (IRMSS)
(12) Space Imaging Ikonos (IK)
(13) Digital Globe QuickBird (QB)
(14) National Polar-orbiting Operational Environmental Satellite System (NPOESS) Visible/Infrared Imager/Radiometer Suite (VIIRS)
(15) National Oceanic and Atmospheric Administration satellite 16 (NOAA-16) Advanced Very High Resolution Radiometer (AVHRR)
(16) Earth Resource Satellite-2 (ERS-2) Along Track Scanning Radiometer-2 (ATSR-2)
(17) Système Pour l'Observation de la Terre-4 (SPOT-4) Vegetation (VGT)
(18) Terra Moderate Resolution Imaging Spectroradiometer (MODIS)
(19) Advanced Earth Observing Satellite-2 (ADEOS-2) Global Imager (GLI)
(20) Terra Multi-angle Imaging Spectro-Radiometer (MISR)

Please cite this article as: Teillet, P. M. et al. Impacts of spectral band difference effects on radiometric cross-calibration between satellite sensors in the solar-reflective spectral domain. *Remote Sensing of Environment* (2007), doi:10.1016/j.rse.2007.03.003

Table 3
Satellite sensors and analogous spectral band numbers, where MS = multi-spectral, NIR = near infrared, SWIR = shortwave-infrared, and MIR = middle infrared

# ID	Satellite sensor	Blue band	Green band	Red band	NIR band	SWIR band I	SWIR band II
1	L7 ETM+	1	2	3	4	5	7
2	L5 TM	1	2	3	4	5	7
3	L4 TM	1	2	3	4	5	7
4	ADEOS-1 AVNIR	1	2	3	4	–	–
5	EO-1 ALI	1	2	3	4p	5	7
6	Terra ASTER	–	1	2	3	4	6
7	SPOT-5 HRG	–	1	2	3	MIR	–
8	IRS-P6 LISS-III	–	2	3	4	5	–
9	IRS-P6 AWiFS	–	2	3	4	5	–
10	CBERS-2 HRCC / IRMSS*	1	2	3	4	2*	3*
11	Ikonos	MS1	MS2	MS3	MS4	–	–
12	Quickbird	MS1	MS2	MS3	MS4	–	–
13	NPOESS VIIRS	M3	M4	I1	I2	I3	M11
14	NOAA-16 AVHRR	–	–	1	2	3A	–
15	ERS-2 ATSR-2	–	1	2	3	MIR	–
16	SPOT-4 VGT	0	–	2	3	MIR	–
17	Terra MODIS	3	4	1	2	6	7
18	ADEOS-2 GLI	20	21	22	23	28	29
19	Terra MISR	1	2	3	4	–	–

SWIR bands I and II are analogous to Landsat bands 5 and 7, respectively. Satellite and sensor acronyms are defined in Table 2. The CBERS-2 HRCC and IRMSS sensors are listed together because their spectral bands taken together map to the Landsat bands.

all other combinations of comparisons between sensors. Twenty Earth observation satellite sensors (including coarser and higher spatial resolution sensors) were considered (Table 2 lists the sensors and their acronyms). The Landsat solar-reflective spectral domain was adopted as the spectral framework for these comparisons (Table 3). Spectral scene content was simulated using ground spectra for four ground target types of interest in the calibration context (Table 4), together with a few combinations of atmospheric states and illumination geometries (observation conditions). Results were obtained as a function of ground target type, satellite sensor comparison, spectral region, and observation conditions.

2. Previous studies on satellite sensor cross-calibration

Teillet et al. (2001b, 2006) reported on a radiometric cross-calibration of the Landsat-7 ETM+ and Landsat-5 Thematic Mapper (TM) sensors based on tandem-orbit data sets. Spectral band difference effects (SBDE) were shown to be significant, despite the close similarity in spectral filters and response functions, and more dependent on the surface reflectance spectrum than on atmospheric and illumination conditions. A variety of terrestrial targets were assessed regarding their suitability for Landsat radiometric cross-calibration in the absence of ground-based reflectance spectra. The combined effort of anchoring Landsat-5 to Landsat-7 radiometry in absolute terms with a detailed retrospective trend analysis of Landsat-5 TM radiometry (Helder et al., 2004) made it possible to establish and implement a definitive calibration record for the lifetime of the Landsat-5 TM (Chander & Markham, 2003; Chander et al., 2004; Teillet et al., 2004).

Trishchenko et al. (2002) focused on moderate resolution satellite sensors, including the Advanced Very High Resolution Radiometers (AVHRR) onboard the NOAA-6,-7,-8,-10,-11,-12,-14,-15,-16 spacecraft, Terra Moderate-resolution Imaging Spectroradiometer (MODIS), SPOT-4 Vegetation (VGT), and Global Imager (GLI) on the second Advanced Earth Observing Satellite (ADEOS-2), all with respect to NOAA-9 AVHRR. They reported on modeling results in the red and near infrared (NIR) and also emphasized the effect of spectral band differences on the Normalized Difference Vegetation Index (NDVI), the most widely used index for vegetation monitoring. They also reported that, without taking spectral band differences into account, reflectance differences range from −25% to +12% in the red and −2% to +4% in the NIR, even between "same type" AVHRR sensors, and that still greater differences can arise for the other sensor inter-comparisons. NDVI differences were found to range from −0.02 to +0.06.

Steven et al. (2003) provided additional background on the problem of inter-calibrating vegetation indices and reported on a simulation study involving red and NIR spectral bands and vegetation indices for 15 satellite sensors. Surface spectral reflectance measurements of agricultural targets were used to generate the results. Conversion coefficients were generated for all sensor combinations and were found to enable inter-sensor NDVI comparisons to a precision of 1% to 2%.

Table 4
The four ground target types used in this study

(1) RVPN: Railroad Valley Playa, Nevada (average of two spectra based on ASD spectrometer data acquired during the TM and ETM+ overpasses on 1999-06-01)
(2) SAND: Desert sand (CAM5S; unchanged from original 5S desert sand spectrum, whose source is cited as being Staetter & Schroeder (1978))
(3) SNOW: Two-day-old snow (O'Brien & Munis, 1975)
(4) NCRA: Newell County Rangeland, Alberta (based on GER spectrometer data acquired on 1997-07-21)

Please cite this article as: Teillet, P. M. et al. Impacts of spectral band difference effects on radiometric cross-calibration between satellite sensors in the solar-reflective spectral domain. *Remote Sensing of Environment* (2007), doi:10.1016/j.rse.2007.03.003

Rao et al. (2003) presented results on the inter-calibration of Terra MODIS and the European Remote Sensing satellite-2 (ERS-2) Along-Track Scanning Radiometer-2 (ATSR-2) based on desert sites as common targets. They emphasized how crucial it is to take into consideration the spectral character of the sensors and the scene to avoid compromising the efficacy of inter-calibration.

3. Assumptions

3.1. Radiometric

- It is assumed that the satellite sensors under consideration have linear radiometric response over the range of relevant radiances.
- Differences in radiometric resolution were not taken into consideration.
- Bidirectional reflectance effects arising from differences in illumination and observation angles were not taken into account. In general, cross-calibration methodologies should consider adjustments for bi-directional reflectance effects. Even if the same target is imaged the same day, significant overpass time and off-nadir viewing angle differences can arise depending on the satellite sensors being compared. The focus in this study is on spectral effects, which arise regardless of geometry effects. Hence, Lambertian reflectance factors are used.
- The terrain is assumed to be flat and horizontal, a good assumption for benchmark sites used for radiometric calibration purposes.

3.2. Spectral

- Given that the Landsat-7 ETM+ is well-calibrated radiometrically, cross-calibration between the ETM+ and the other imaging sensors was the starting point for the study. With SBDEs on cross-calibration between ETM+ and other sensors in hand, it was straightforward to examine all other combinations between sensors (in spectral bands with analogs to one or more of the six solar-reflective Landsat bands). The analogous spectral bands are identified in Table 3 for the Earth observation satellite sensors involved. There may some day be a better set of satellite sensor spectral bands to use as the framework for multiple cross-calibration comparisons, but for now the Landsat-centric perspective is retained.
- It is assumed that the spectral bands were well characterized prior to launch and that they remain unchanged post-launch. Once a given satellite sensor is in orbit, it is difficult to assess changes in the sensor's spectral characteristics.[1] Relatively few investigations have addressed the evaluation and impact of post-launch changes in spectral band characteristics (Flittner and Slater, 1991; Suits et al., 1988; Teillet, 1997, 1990; Teillet et al., 1997b).
- Out-of-band response (i.e., contributions not included in the relative spectral response profiles provided by the agencies responsible for the sensors) is not taken into consideration. Even if the nominal spectral bands being compared are almost identical, the out-of-band response can still differ significantly between imaging sensors.

3.3. Spatial

- This simulation study involves point calculations and, hence, spatial considerations are not a concern. Typically, cross-calibration analyses that involve image data are designed to avoid susceptibility to possible spatial misregistration of images over common ground targets (Teillet et al., 2001b, 2006). Even for relatively uniform targets, pixel-specific comparisons are avoided.

3.4. Temporal

- This simulation study involves steady-state model calculations and, hence, temporal considerations are not involved. Typically, cross-calibrations between satellite sensors utilize imagery of common ground targets acquired within a short space of time. Ideally, "a short space of time" in this context implies within minutes in order to avoid variable solar illumination and atmospheric conditions. In practice, calibration data sets are typically acquired on very clear days and so same-day comparisons with sun-angle corrections are acceptable within a framework of systematic monitoring of imaging sensor calibration performance. Attempts to cross-calibrate multiple satellite sensors imaging a target one or more days apart can yield mixed results (Teillet et al., 2001c).

4. Radiometric formulation

The key radiometric equations for top-of-atmosphere (TOA) quantities are as follows (Teillet et al., 2001b). For a given spectral band:

$$\text{Image quantized level (in counts)} = Q_\mathrm{i} = G_\mathrm{i} L_\mathrm{i}^* + Q_{0\mathrm{i}}, \tag{1}$$

$$\text{At-sensor radiance (in Watts/(m}^2 sr\mu m)) = L_\mathrm{i}^* = (Q_\mathrm{i} - Q_{0\mathrm{i}})/G_\mathrm{i} = \Delta Q_\mathrm{i}/G_\mathrm{i}, \tag{2}$$

$$\text{At-sensor reflectance} = \rho_\mathrm{i}^* = \pi L_\mathrm{i}^* d_\mathrm{s}^2/(E_{0\mathrm{i}} \cos\theta). \tag{3}$$

In these equations, G_i is band-averaged sensor responsivity (in counts per unit radiance) and $Q_{0\mathrm{i}}$ is the band-averaged zero-radiance bias (in counts), in spectral band i. Also, $E_{0\mathrm{i}}$ is the exo-atmospheric solar irradiance (in Watts/(m^2 μm)), θ is the solar zenith angle, and d_s is the Earth–Sun distance in Astronomical Units. Bias-corrected image values are then given by

$$\Delta Q_\mathrm{i} = Q_\mathrm{i} - Q_{0\mathrm{i}} = G_\mathrm{i} \rho_\mathrm{i}^* E_{0\mathrm{i}} \cos\theta/(\pi d_\mathrm{s}^2). \tag{4}$$

[1] The Terra MODIS includes a sub-system called the Spectroradiometric Calibration Assembly (SRCA), which has been used to confirm that the MODIS spectral bands have not changed significantly since launch (Che et al., 2003).

Please cite this article as: Teillet, P. M. et al. Impacts of spectral band difference effects on radiometric cross-calibration between satellite sensors in the solar-reflective spectral domain. *Remote Sensing of Environment* (2007), doi:10.1016/j.rse.2007.03.003

There are two advantages to using reflectances instead of radiances. One advantage is to allow for the cosine effect of different solar zenith angles due to the time difference between data acquisitions. The other advantage is to compensate for different values of exo-atmospheric solar irradiance arising from spectral band differences.

4.1. Cross-calibration for raw data

Radiometric calibration specialists often use raw (Level-0) data and seek to update responsivity coefficients for the imaging sensors under consideration. The following formulation is developed accordingly. Eq. (4) can be defined separately for image data from a reference sensor ("R") and for image data from another sensor ("X"), whose calibration is to be checked via cross-calibration with respect to sensor R in analogous spectral band i. After algebraic manipulation, this leads to

$$\Delta Q_{\mathrm{iXA}} = A_{\mathrm{i}}\ \Delta Q_{\mathrm{iX}} = (G_{\mathrm{iX}}/G_{\mathrm{iR}})\ \Delta Q_{\mathrm{iR}} = M_{\mathrm{i}}\Delta Q_{\mathrm{iR}}, \tag{5}$$

where the factor A_{i} adjusts sensor X radiances for illumination and spectral band difference effects and M_{i} is the slope of the linear equation that characterizes ΔQ_{iXA} as a function of ΔQ_{iR}. In particular,

$$A_{\mathrm{i}} = B_{\mathrm{i}}(E_{0\mathrm{i}}\cos\theta)_{\mathrm{R}}/(E_{0\mathrm{i}}\cos\theta)_{\mathrm{X}}, \tag{6}$$

where

$$B_{\mathrm{i}} = \rho^*_{\mathrm{iR}}/\rho^*_{\mathrm{iX}}. \tag{7}$$

B_{i} is essentially a spectral band adjustment factor, given that ρ^*_{iX} and ρ^*_{iR} are not the same because of the differences in relative spectral response profiles between corresponding (analogous) spectral bands. Sensor X responsivity G_{iX} in spectral band i is then given (in counts per unit radiance) by

$$G_{\mathrm{iX}} = M_{\mathrm{i}}\ G_{\mathrm{iR}}. \tag{8}$$

Thus, nearly coincident (same-day) data acquisitions over common targets make it possible to use image data from well-calibrated sensors to update the radiometric calibration of other sensors in analogous spectral bands. One of the keys is to have sufficient knowledge of the spectral band adjustment factor B_{i}, since uncertainty in the cross-calibration due to this effect is directly proportional to the uncertainty in B_{i}.

4.2. Cross-calibration for nominally calibrated data

Still in the context of imaging common ground-look targets, another mode of cross-calibration is the comparison of calibrated radiances from different sensors. In this instance, Eq. (3) can be defined separately for radiances from the reference sensor ("R") and the other sensor ("X") such that, after some manipulation,

Table 5
Conditions and parameters involved in TOA reflectance simulations carried out to assess spectral band difference effects

Aerosol optical depth at 0.55 μm (AOD55)	0.05; 0.5
Atmospheric model	US62*: $U(H_2O)=1.424$ g/cm^2 $U(O_3)=0.344$ cm-atm Tropical: $U(H_2O)=4.12$ g/cm^2 $U(O_3)=0.247$ cm-atm *Mid-latitude winter for snow target: $U(H_2O)=0.853$ g/cm^2 $U(O_3)=0.395$ cm-atm
Solar zenith angle (SZA)	15°; 60°
Ground target reflectance spectrum	Railroad Valley Playa, Nevada (RVPN) Desert sand (SAND) Two-day-old snow (SNOW) Newell County Rangeland, Alberta (NCRA)
Conditions common to all cases	Sea-level terrain elevation Nadir viewing geometry Earth–Sun distance=1 A.U. Continental aerosol model

$U(H_2O)$=water vapour content. $U(O_3)$=ozone content. A.U.=Astronomical Units.

$$L^*_{\mathrm{iXA}} = A_{\mathrm{i}}\ L^*_{\mathrm{iX}} = L^*_{\mathrm{iR}}, \tag{9}$$

where A_{i} is the same adjustment factor as defined before in Eq. (6). Given TOA radiances L^*_{iR} from sensor R, Eq. (9) implies that TOA radiances at the entrance aperture of sensor X in analogous spectral band i should be L^*_{iXA}. However, the calibrated image product for sensor X will have TOA radiances L^*_{iXNA} for the common ground target, based on the nominal calibration used to generate that product. L^*_{iXNA} and L^*_{iXA} will differ if the radiometric calibration of sensor X has drifted.

Thus, plots of L^*_{iR} versus L^*_{iXNA}, i.e., the radiances from the image data acquired by the two sensors over the common ground target, yield

$$L^*_{\mathrm{iR}} = m_{\mathrm{i}}L^*_{\mathrm{iXNA}} + b_{\mathrm{i}}, \tag{10}$$

where m_{i} and b_{i} are the slope and intercept, respectively. Assuming a linear calibration change for sensor X, one can define the relationship between nominally calibrated radiances and cross-calibrated radiances as follows:

$$L^*_{\mathrm{iX}} = \alpha_{\mathrm{i}}\ L^*_{\mathrm{iXN}} + \beta_{\mathrm{i}}. \tag{11}$$

Based on the combination of Eqs. (9), (10), and (11),

$$\alpha_{\mathrm{i}} = m_{\mathrm{i}} \tag{12}$$

and

$$\beta_{\mathrm{i}} = b_{\mathrm{i}}/A_{\mathrm{i}}. \tag{13}$$

Please cite this article as: Teillet, P. M. et al. Impacts of spectral band difference effects on radiometric cross-calibration between satellite sensors in the solar-reflective spectral domain. *Remote Sensing of Environment* (2007), doi:10.1016/j.rse.2007.03.003

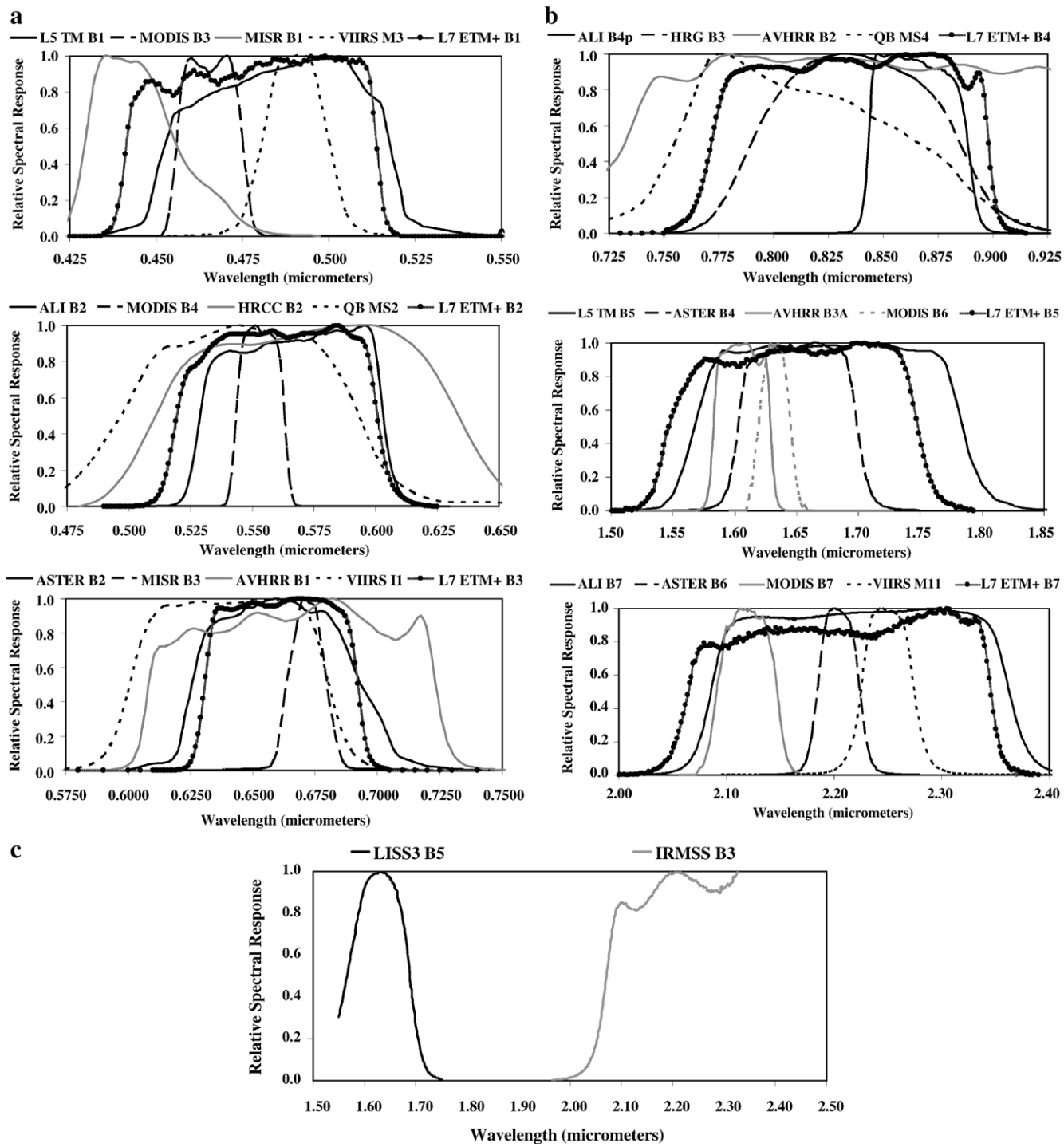

Fig. 1. (a) Examples of satellite sensor spectral bands analogous to Landsat ETM+ band 1 (top), band 2 (middle) and band 3 (bottom). (b) Examples of satellite sensor spectral bands analogous to Landsat ETM+ band 4 (top), band 5 (middle) and band 7 (bottom). (c) Incomplete relative spectral response functions for LISS-III band 5 (Landsat band 5 analog) and IRMSS band 3 (Landsat band 7 analog).

Thus, nearly coincident (same-day) data acquisitions over common targets make it possible to generate a radiance calibration update equation for data from sensor "X" (Eq. (11)). Note that adjustment factor A_i is involved and, hence, so is the spectral band adjustment factor B_i , which is the focus of the work reported in this paper.

5. Methodology

5.1. Generation of spectral band adjustment factors

The key parameter to be computed is the spectral band adjustment factor B_i (Eq. (7)) in a given spectral band i, which is a

Please cite this article as: Teillet, P. M. et al. Impacts of spectral band difference effects on radiometric cross-calibration between satellite sensors in the solar-reflective spectral domain. *Remote Sensing of Environment* (2007), doi:10.1016/j.rse.2007.03.003

function of TOA reflectances and hence scene content. Scene content was simulated using the ground target spectra listed in Table 4 and described below, together with selected atmospheric states and illumination and viewing geometries listed in Table 5. To compute the TOA reflectances and thence the B_i factors, the surface reflectance spectrum for each ground target was used as input to an atmospheric radiative transfer code to calculate the TOA reflectances in corresponding solar reflective spectral bands for all of the imaging sensors considered (Tables 2 and 3). The atmospheric code is the Canadian Advanced Modified 5S (CAM5S) code.[2] Results for B_i were obtained as a function of calibration target, satellite sensor, spectral region, and scene content.

5.2. Spectral bands

Because there are many sensor spectral bands in each Landsat analog spectral region, it is not easy to show them all in the same plot. Fig. 1a and b shows examples that are meant to be roughly representative of the gamut of similar relative spectral response profiles from the sensors not shown. The plots in Fig. 1 clearly illustrate how different the various satellite sensor spectral bands can be, despite being in the same region of the electromagnetic spectrum.

Band 1 The L5 TM profile is roughly representative of the blue bands of L4 TM, ALI, IK, QB and HRCC. The VGT profile is somewhat like the MODIS profile shown in the figure.

Band 2 The ALI profile is roughly representative of the green bands of L4 TM, L5 TM, ASTER and LISS-III. The VGT profile is somewhat like the MODIS profile shown in the figure. The ATSR-2, MISR and VIIRS profiles are somewhat like the MODIS profile shown in the figure. The HRG and IK profiles are represented by the QB profile.

Band 3 The ASTER profile is roughly representative of the red bands of L4 TM, L5 TM, ALI, HRG, VGT, HRCC, IK, QB and LISS-III. The ATSR-2 profile is somewhat like the MISR profile shown in the figure.

Band 4 The ALI profile is roughly representative of the near-infrared bands of ATSR-2, MODIS, MISR and VIIRS. The HRG profile represents L4 TM, L5 TM, VGT and HRCC. The ATSR-2 profile is somewhat like the MISR profile shown in the figure. The ASTER and IK profiles are represented by the QB profile.

Band 5 The ASTER profile is roughly representative of the SWIR Band I profiles of HRG, VGT and LISS-III. The ALI profile is somewhat like the L7 ETM+ profile shown in the figure. The L5 TM profile represents the L4 TM and IRMSS profiles. The AVHRR profile represents the ATSR-2 and VIIRS profiles.

Band 7 The ALI profile is roughly representative of the SWIR Band II profiles of all other sensors not shown in the figure.

It should be noted that the available relative spectral response functions for LISS-III band 5 (Landsat band 5 analog) and IRMSS band 3 (Landsat band 7 analog) are incomplete (Fig. 1c) such that the results in these bands will be off slightly.

5.3. Ground targets

5.3.1. RVPN

The test site at Railroad Valley Playa, Nevada (RVPN) is one of the most extensively used optical calibration test sites in the world. The surface reflectance spectrum used here (Fig. 2) is the average of two spectra obtained from data acquired during the TM and ETM+ overpasses June 1, 1999 using portable Analytical Spectral Devices (ASD) spectrometers. The RVPN target is a dry-lake playa that is very homogeneous and consists of compacted clay-rich lacustrine deposits forming a relatively smooth surface compared to most land covers.

5.3.2. SAND

The sand spectrum from the 5S series of atmospheric codes was selected to represent the desert calibration areas often used for ground-look calibration. The 5S code cites Staetter & Schroeder (1978) as the source of this spectrum.

5.3.3. SNOW

A snow spectrum was used to represent the snow areas occasionally used for ground-look calibration. In particular, a two-day-old snow spectrum was selected as opposed to fresh snow. The spectrum was obtained from O'Brien & Munis (1975).

5.3.4. NCRA

A semi-arid region of rangeland in Newell County, Alberta (NCRA) has been considered as a potential calibration site (Teillet et al., 1998, 1999). The area is characterised by short

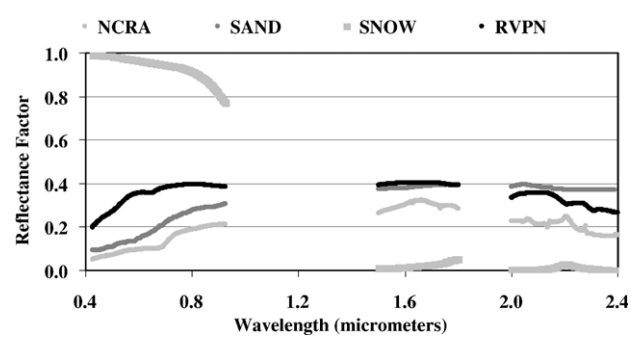

Fig. 2. Surface reflectance spectra for the indicated ground targets in the Landsat solar-reflective spectral bands.

[2] CAM5S is a descendent of the 5S code (Simulation of the Satellite Signal in the Solar Spectrum) (Tanré et al., 1990). Some years ago, terrain elevation and sensor altitude dependence capabilities were added to the original 5S (Teillet and Santer, 1991), renamed H5S at that time. Other new features were subsequently added to H5S, which became CAM5S (O'Neill et al., 1996), which includes other improvements adopted from the 6S (Second 5S) code developed by Vermote et al. (1997). For the cases examined here, CAM5S and 6S should yield the same results (6S would be better for larger illumination and observation angles). CAM5S was retained because multiple run scripts and associated software tools have been developed over the time and because the CAM5S code is much cleaner and better documented than the 6S code.

Please cite this article as: Teillet, P. M. et al. Impacts of spectral band difference effects on radiometric cross-calibration between satellite sensors in the solar-reflective spectral domain. *Remote Sensing of Environment* (2007), doi:10.1016/j.rse.2007.03.003

Table 6

Sensor Spectral Bands																			
ETM+ Band 1 Analogs	1	2	3	4	5	6	7	8	9	10	11	12	13	14	15	16	17	18	19
1: Landsat-7 ETM+ B1		-0.7	-0.7	0.9	-0.5					-1.3	-1.0	-0.5	-0.9			1.5	0.5	1.1	2.5
2: Landsat-5 TM B1			0.0	1.6	0.2					-0.6	-0.3	0.2	-0.2			2.2	1.2	1.8	3.2
3: Landsat-4 TM B1				1.6	0.2					-0.6	-0.3	0.2	-0.2			2.2	1.2	1.8	3.2
4: ADEOS-1 AVNIR B1					-1.4					-2.2	-1.8	-1.4	-1.8			0.6	-0.3	0.2	1.6
5: EO-1 ALI B1										-0.8	-0.5	0.0	-0.4			2.0	1.0	1.6	3.0
6: Terra ASTER N/A																			
7: SPOT-5 HRG-1 N/A																			
8: IRS-P6 LISS-III N/A																			
9: IRS-P6 AWiFS N/A																			
10: CBERS-2 HRCC B1											0.4	0.8	0.4			2.8	1.9	2.4	3.9
11: Ikonos MS1												0.5	0.0			2.5	1.5	2.1	3.5
12: QuickBird MS1													-0.4			2.0	1.0	1.6	3.0
13: NPOESS VIIRS M3																2.4	1.5	2.0	3.5
14: NOAA-16 AVHRR N/A																			
15: ERS-2 ATSR-2 N/A																			
16: SPOT-4 VGT B0																	-0.9	-0.4	1.0
17: Terra MODIS B3																		0.5	2.0
18: ADEOS-2 GLI B20																			1.4
19: Terra MISR B1																			

ETM+ Band 2 Analogs	1	2	3	4	5	6	7	8	9	10	11	12	13	14	15	16	17	18	19
1: Landsat-7 ETM+ B2		-0.7	-0.7	0.1	-0.4	0.5	1.2	-0.2	-0.2	-1.2	0.6	1.4	-1.0		-1.0		-1.0	0.6	-1.1
2: Landsat-5 TM B2			0.0	0.8	0.2	1.2	1.8	0.5	0.5	-0.6	1.3	2.0	-0.3		-0.4		-0.3	1.2	-0.4
3: Landsat-4 TM B2				0.8	0.2	1.2	1.8	0.5	0.5	-0.6	1.3	2.0	-0.3		-0.4		-0.3	1.2	-0.4
4: ADEOS-1 AVNIR B2					-0.5	0.4	1.1	-0.3	-0.3	-1.3	0.5	1.3	-1.1		-1.1		-1.1	0.5	-1.2
5: EO-1 ALI B2						0.9	1.6	0.2	0.2	-0.8	1.0	1.8	-0.6		-0.6		-0.6	1.0	-0.7
6: Terra ASTER B1							0.7	-0.7	-0.7	-1.7	0.1	0.9	-1.5		-1.5		-1.5	0.1	-1.6
7: SPOT-5 HRG-1 B1								-1.4	-1.4	-2.4	-0.6	0.2	-2.1		-2.2		-2.1	-0.6	-2.2
8: IRS-P6 LISS-III B2									0.0	-1.0	0.8	1.6	-0.8		-0.8		-0.8	0.8	-0.9
9: IRS-P6 AWiFS B2										-1.0	0.8	1.6	-0.8		-0.8		-0.8	0.8	-0.9
10: CBERS-2 HRCC B2											1.9	2.6	0.3		0.2		0.3	1.8	0.2
11: Ikonos MS2												0.8	-1.6		-1.6		-1.6	0.0	-1.7
12: QuickBird MS2													-2.3		-2.4		-2.3	-0.8	-2.4
13: NPOESS VIIRS M4															-0.1		0.0	1.6	-0.1
14: NOAA-16 AVHRR N/A																			
15: ERS-2 ATSR-2 B1																	0.1	1.6	0.0
16: SPOT-4 VGT N/A																			
17: Terra MODIS B4																		1.6	-0.1
18: ADEOS-2 GLI B21																			-1.6
19: Terra MISR B2																			

vegetation cover with limited phenological activity, terrain that is flat to very gently rolling, and a surface reflectance that is lower compared to playa and desert sites at most wavelengths. Although the ground cover is spatially heterogeneous at detailed scales, it is relatively homogeneous at the pixel scales of the imaging satellite sensors of interest. The surface reflectance spectrum used here (Fig. 2) was obtained from data acquired on July 21, 1997 using a GER3700 spectrometer.

5.4. Atmospheric states and general observation conditions

5.4.1. Aerosol optical depth

The atmospheric aerosol optical depth (AOD) has a weak spectral dependence and so it is not expected to play a significant role in SBDEs. Nevertheless, two cases were considered to confirm this expectation: AOD at 0.55 μm (AOD55) = 0.05 and 0.5.

5.4.2. Atmospheric model

The choice of atmospheric model dictates the atmospheric temperature and pressure profiles as a function of altitude, as well as atmospheric gas contents for O_2, H_2O, O_3, CO_2 and CH_4. Among the various standard models available in CAM5S, two were selected to represent a typical atmosphere (US62) and a more humid atmosphere (Tropical) (Table 5). For model runs involving the SNOW ground target, the mid-latitude winter atmospheric model was used instead of US62 and comparisons with respect to the Tropical results were not considered.

5.4.3. Solar Zenith Angle

Differences in the solar zenith angle (SZA) are not expected to be an important factor, even though they involve different path lengths through the atmosphere. Nevertheless, results were

Please cite this article as: Teillet, P. M. et al. Impacts of spectral band difference effects on radiometric cross-calibration between satellite sensors in the solar-reflective spectral domain. *Remote Sensing of Environment* (2007), doi:10.1016/j.rse.2007.03.003

Table 6 (*continued*)

Sensor Spectral Bands																			
ETM+ Band 3 Analogs	1	2	3	4	5	6	7	8	9	10	11	12	13	14	15	16	17	18	19
1: Landsat-7 ETM+ B3		0.2	0.2	1.3	-0.2	0.1	0.6	0.4	0.1	0.1	0.1	0.9	2.1	0.8	-0.1	0.3	-0.3	-0.2	-5.0
2: Landsat-5 TM B3			0.0	1.1	-0.4	-0.1	0.4	0.2	-0.1	-0.1	-0.1	0.7	1.9	0.6	-0.3	0.1	-0.5	-0.4	-5.2
3: Landsat-4 TM B3				1.1	-0.4	-0.1	0.4	0.2	-0.1	-0.1	-0.1	0.7	1.9	0.6	-0.3	0.1	-0.5	-0.4	-5.2
4: ADEOS-1 AVNIR B3					-1.5	-1.2	-0.7	-0.8	-1.2	-1.2	-1.2	-0.3	0.8	-0.4	-1.4	-0.9	-1.5	-1.4	-6.2
5: EO-1 ALI B3						0.3	0.8	0.6	0.3	0.3	0.3	1.2	2.3	1.1	0.1	0.5	-0.1	0.1	-4.8
6: Terra ASTER B2							0.5	0.3	0.0	0.0	0.0	0.8	2.0	0.8	-0.2	0.2	-0.4	-0.2	-5.1
7: SPOT-5 HRG-1 B2								-0.2	-0.5	-0.5	-0.5	0.3	1.5	0.2	-0.7	-0.3	-0.9	-0.8	-5.6
8: IRS-P6 LISS-III B3									-0.3	-0.3	-0.3	0.5	1.7	0.4	-0.5	-0.1	-0.7	-0.6	-5.4
9: IRS-P6 AWiFS B3										0.0	0.0	0.8	2.0	0.8	-0.2	0.2	-0.4	-0.2	-5.1
10: CBERS-2 HRCC B3											0.0	0.8	2.0	0.8	-0.2	0.2	-0.4	-0.2	-5.1
11: Ikonos MS3												0.8	2.0	0.8	-0.2	0.2	-0.4	-0.2	-5.1
12: QuickBird MS3													1.2	-0.1	-1.1	-0.6	-1.2	-1.1	-5.9
13: NPOESS VIIRS I1														-1.2	-2.2	-1.7	-2.3	-2.2	-7.0
14: NOAA-16 AVHRR B1															-1.0	-0.5	-1.1	-1.0	-5.8
15: ERS-2 ATSR-2 B2																0.5	-0.1	0.0	-4.9
16: SPOT-4 VGT B2																	-0.6	-0.5	-5.3
17: Terra MODIS B1																		0.1	-4.7
18: ADEOS-2 GLI B22																			-4.9
19: Terra MISR B3																			

ETM+ Band 4 Analogs	1	2	3	4	5	6	7	8	9	10	11	12	13	14	15	16	17	18	19
1: Landsat-7 ETM+ B4		1.6	1.6	2.6	-5.3	3.7	1.1	0.7	0.4	2.0	4.2	3.8	-4.3	14.3	-5.7	1.6	-3.9	0.3	-5.2
2: Landsat-5 TM B4			0.0	1.0	-6.7	2.1	-0.4	-0.8	-1.2	0.4	2.6	2.2	-5.7	12.6	-7.2	0.0	-5.4	-1.3	-6.6
3: Landsat-4 TM B4				1.0	-6.7	2.1	-0.4	-0.8	-1.2	0.4	2.6	2.2	-5.7	12.6	-7.2	0.0	-5.4	-1.3	-6.6
4: ADEOS-1 AVNIR B4					-7.6	1.1	-1.4	-1.8	-2.2	-0.6	1.6	1.2	-6.7	11.5	-8.1	-1.0	-6.3	-2.2	-7.5
5: EO-1 ALI B4p						9.5	6.8	6.3	5.9	7.6	10.0	9.5	1.1	20.7	-0.5	7.2	1.5	5.8	0.1
6: Terra ASTER B3							-2.5	-2.9	-3.2	-1.7	0.5	0.1	-7.7	10.2	-9.1	-2.1	-7.3	-3.3	-8.6
7: SPOT-5 HRG-1 B3								-0.4	-0.8	0.8	3.0	2.6	-5.3	13.0	-6.8	0.4	-5.0	-0.9	-6.2
8: IRS-P6 LISS-III B4									-0.4	1.2	3.5	3.0	-5.0	13.5	-6.4	0.8	-4.6	-0.4	-5.8
9: IRS-P6 AWiFS B4										1.6	3.8	3.4	-4.6	13.9	-6.0	1.2	-4.2	-0.1	-5.5
10: CBERS-2 HRCC B4											2.2	1.8	-6.1	12.1	-7.5	-0.4	-5.7	-1.7	-7.0
11: Ikonos MS4												-0.4	-8.1	9.7	-9.5	-2.5	-7.8	-3.8	-9.0
12: QuickBird MS4													-7.7	10.2	-9.1	-2.1	-7.4	-3.4	-8.6
13: NPOESS VIIRS I2														19.4	-1.5	6.1	0.4	4.7	-0.9
14: NOAA-16 AVHRR B2															-17.5	-11.2	-15.9	-12.3	-17.0
15: ERS-2 ATSR-2 B3																7.7	1.9	6.3	0.6
16: SPOT-4 VGT B3																	-5.4	-1.3	-6.6
17: Terra MODIS B2																		4.3	-1.3
18: ADEOS-2 GLI B23																			-5.4
19: Terra MISR B4																			

(continued on next page)

generated for two cases to confirm this expectation: SZA = 15° and 60°.

5.4.4. Other conditions

The following conditions were common to all cases considered in the study: sea-level terrain elevation, nadir viewing geometry, Earth–Sun distance of 1 Astronomical Unit (A.U.), and a standard continental aerosol model.

6. Results for Railroad Valley Playa

The modeling results for the RVPN site are presented in the form of matrices of the SBDE for all sensor spectral band combinations (Table 6). Specifically, the results are tabulated in terms of percent relative difference due to uncorrected SBDE, S, defined as follows:

$$S = 100(B_i - 1)\%. \tag{14}$$

Because uncorrected SBDEs are but one of several sources of sensor cross-calibration uncertainty, one would like them to be small, within ±3% say. Hence, "good" results are considered to be those where S is within ±3%. In such cases, uncertainty due to lack of knowledge about the spectral content of the scene is comparable to other uncertainties involved in the cross-calibration (Biggar et al., 1994).

Please cite this article as: Teillet, P. M. et al. Impacts of spectral band difference effects on radiometric cross-calibration between satellite sensors in the solar-reflective spectral domain. *Remote Sensing of Environment* (2007), doi:10.1016/j.rse.2007.03.003

Table 6 (*continued*)

Sensor Spectral Bands																			
ETM+ Band 5 Analogs	**1**	**2**	**3**	**4**	**5**	**6**	**7**	**8**	**9**	**10**	**11**	**12**	**13**	**14**	**15**	**16**	**17**	**18**	**19**
1: Landsat-7 ETM+ B5	1	5.2	5.2		-1.1	-2.4	-2.1	-2.0	-1.9	2.2			-2.2	-2.5	-1.9	-1.8	-2.8	-0.4	
2: Landsat-5 TM B5		1	0.0		-6.0	-7.3	-6.9	-6.9	-6.8	-2.8			-7.0	-7.3	-6.8	-6.7	-7.6	-5.3	
3: Landsat-4 TM B5			1		-6.0	-7.3	-6.9	-6.9	-6.8	-2.8			-7.0	-7.3	-6.8	-6.7	-7.6	-5.3	
4: ADEOS-1 AVNIR N/A																			
5: EO-1 ALI B5					1	-1.4	-1.0	-0.9	-0.8	3.3			-1.1	-1.4	-0.9	-0.7	-1.7	0.7	
6: Terra ASTER B4						1	0.4	0.4	0.6	4.8			0.3	0.0	0.5	0.7	-0.3	2.1	
7: SPOT-5 HRG-1 MIR							1	0.1	0.2	4.4			-0.1	-0.4	0.1	0.3	-0.7	1.7	
8: IRS-P6 LISS-III B5								1	0.1	4.3			-0.2	-0.4	0.1	0.2	-0.8	1.7	
9: IRS-P6 AWiFS B5									1	4.2			-0.3	-0.6	-0.1	0.1	-0.9	1.5	
10: CBERS-2 IRMSS B2										1			-4.3	-4.6	-4.1	-3.9	-4.9	-2.5	
11: Ikonos N/A																			
12: QuickBird N/A																			
13: NPOESS VIIRS I3													1	-0.3	0.2	0.4	-0.6	1.8	
14: NOAA-16 AVHRR B3A														1	0.5	0.7	-0.3	2.1	
15: ERS-2 ATSR-2 MIR															1	0.2	-0.8	1.6	
16: SPOT-4 VGT MIR																1	-1.0	1.4	
17: Terra MODIS B6																	1	2.5	
18: ADEOS-2 GLI B28																		1	
19: Terra MISR N/A																			

ETM+ Band 7 Analogs	**1**	**2**	**3**	**4**	**5**	**6**	**7**	**8**	**9**	**10**	**11**	**12**	**13**	**14**	**15**	**16**	**17**	**18**	**19**
1: Landsat-7 ETM+ B7	1	-5.6	-5.6		-4.3	-6.2				-6.3			-3.7				-20.5	-10.7	
2: Landsat-5 TM B7		1	0.0		1.4	-0.6				-0.7			2.1				-15.7	-5.3	
3: Landsat-4 TM B7			1		1.4	-0.6				-0.7			2.1				-15.7	-5.3	
4: ADEOS-1 AVNIR N/A																			
5: EO-1 ALI B7					1	-2.0				-2.1			0.7				-16.9	-6.7	
6: Terra ASTER B6						1				-0.1			2.7				-15.2	-4.8	
7: SPOT-5 HRG-1 N/A																			
8: IRS-P6 LISS-III N/A																			
9: IRS-P6 AWiFS N/A																			
10: CBERS-2 IRMSS B3										1			2.8				-15.2	-4.7	
11: Ikonos N/A																			
12: QuickBird N/A																			
13: NPOESS VIIRS M11													1				-17.5	-7.3	
14: NOAA-16 AVHRR N/A																			
15: ERS-2 ATSR-2 N/A																			
16: SPOT-4 VGT N/A																			
17: Terra MODIS B7																	1	12.3	
18: ADEOS-2 GLI B29																		1	
19: Terra MISR N/A																			

(a) Analog spectral band 1 and band 2 results (US62, AOD55 = 0.05, and SZA = 60°) for uncorrected SBDEs on cross-calibration between sensors using RVPN as the common ground target. Cells with S values (Eq. (14)) within ±3% are white, >+3% light grey, and <−3% dark grey.
(b) Analog spectral band 3 and band 4 results (US62, AOD55 = 0.05, and SZA = 60°) for uncorrected SBDEs on cross-calibration between sensors using RVPN as the common ground target. Cells with S values (Eq. (14)) within ±3% are white, >+3% light grey, and <−3% dark grey.
(c) Analog spectral band 5 and band 7 results (with US62, AOD55 = 0.05, and SZA = 60°) for uncorrected SBDEs on cross-calibration between sensors using RVPN as the common ground target. Cells with S values (Eq. (14)) within ±3% are white, >+3% light grey, and <−3% dark grey.

Table 6 presents the RVPN results for US62, AOD55 = 0.05, and SZA = 60°. Highlights are as follows.

Band 1 All sensor combinations are good except for cross-calibration between Terra MISR and several other sensors, although $|S|$ results are within 4% even in those cases.

Band 2 All sensor combinations are good.

Band 3 All sensor combinations are good except for cross-calibration between Terra MISR and all other sensors. In these cases, S is typically −5% and the worst case is −7%.

Band 4 For the finer spatial resolution sensor comparisons, the majority of cases are good. Cross-calibrations between EO-1 ALI and the other higher spatial resolution sensors

are poor, with S ranging from 5.9% to 10%. For the coarser resolution sensor comparisons, less than half of the cases are good, with S as high as 19.4%. For comparisons between finer and coarser spatial resolution sensors, few cases are good. The worst case involves NOAA-16 AVHRR, with S ranging from 9.7% to 20.7%.

Band 5 The results are generally good. Problem cases include Landsat-5 TM, Landsat-4 TM and CBERS-2 IRMSS with respect to almost all of the other sensors. In these cases, $|S|$ results are within 8%.

Band 7 Less than half of the results are good. Problem cases include Landsat-7 ETM+, Terra MODIS, and ADEOS-2 GLI with respect to all of the other sensors. S results involving Landsat-7 ETM+ are within −6.3% except for the Terra MODIS and ADEOS-2 GLI comparisons, which are −20.5% and −10.7%, respectively. S results involving Terra MODIS and ADEOS-2 GLI range from −4.7% to −20.5%, except for the specific MODIS versus GLI comparison, for which S is 12.3%.

7. Results for other ground targets

Model result matrices were also generated for the other ground targets (SAND, SNOW, and NCRA), but these S result tables are not presented here to save space. Highlights of the SAND, SNOW and NCRA results for US62, AOD55 = 0.05, and SZA = 60° are as follows.

7.1. Highlights of results for SAND

Band 1 For the finer spatial resolution sensor comparisons, all results are good except for cross-calibrations between ADEOS-1 AVNIR and all other sensors. In these cases, $|S|$ results are within 6.5%. For the rest of the comparisons, there are few good cases. Problem cases include SPOT-4 VGT, ADEOS-2 GLI, and Terra MISR with respect to almost all other sensors, with S reaching −12.6%.

Band 2 Almost all results are good. The main exception is for CBERS-2 HRCC, but S results are still within 4.5%.

Band 3 The results are generally good. The few exceptions involve ADEOS-1 AVNIR, NPOESS VIIRS, and Terra MISR, the worst being MISR, for which there are no good matches and S is typically −8% and the worst case is −13.5%.

Band 4 The results are very similar to those for RVPN, but with a few more poor cases and with slightly higher $|S|$ values overall.

Band 5 The results are very similar to those for RVPN, but with a few less poor cases and with slightly lower $|S|$ values overall.

Band 7 The results are almost all bad, with S reaching as high as 30%. The only exceptions are Landsat-5 TM versus Landsat-4 TM (S = 0.1), Terra ASTER versus NPOESS VIIRS (S = 2.5), and NPOESS VIIRS versus ADEOS-2 GLI (S = 1.2).

7.2. Highlights of results for SNOW

Band 1 All sensor combinations are good. Indeed, most S results are close to zero and all are within ±1.3%.

Band 2 Almost all results are good. The few exceptions are the cases involving SPOT-5 HRG, QuickBird, and ADEOS-2 GLI with respect to Landsat-5 TM, Landsat-4 TM, and EO-1 ALI, all of which nevertheless have $|S|$ results within 4.1%.

Band 3 The results are all good except for cross-calibrations between Terra MISR and almost all other sensors, for which the $|S|$ results are within 4.6%.

Band 4 For the finer spatial resolution sensor comparisons, all but three cases are good and the exceptions have $|S|$ results within 3.3%. For the rest of the comparisons, the only problem cases are NOAA-16 AVHRR, which has poor $|S|$ results with respect to all other sensors (12% to 16%), and ERS-2 ATSR-2, which has several cases with S between −3% and −4% and S = −14.1% with respect to AVHRR.

Band 5 There are very few good cases and the $|S|$ results reach as high as 35%. Snow spectral reflectance is low in this spectral region such that percent relative differences tend to be high.

Band 7 Except for Landsat-5 TM versus Landsat-4 TM (S = 0.0), the results are all bad, with some S results reaching over 100%. As for band 5, snow spectral reflectance is low in band 7 such that percent relative differences tend to be high.

7.3. Highlights of results for NCRA

Band 1 The results are very similar to those for SAND, but with a few more poor cases and with slightly higher S values overall.

Band 2 Most of the results are good. The exceptions are some cases involving SPOT-5 HRG, Ikonos, QuickBird, and ADEOS-2 GLI, for which the highest $|S|$ result is 5.3%.

Band 3 The results are all good except for cross-calibrations between NOAA-16 AVHRR and some of the other sensors. In these cases, the $|S|$ results are all within 3.3%, except for the NPOESS VIIRS case at 3.7%.

Band 4 The results are very similar to those for SAND, with essentially the same distribution of good and poor cases across all sensor comparisons.

Band 5 The results are mixed, about half of them good. Problem cases mainly involve the Landsat sensors, CBERS-2 IRMSS, and Terra MODIS. In these cross-calibration cases, the $|S|$ results range from 3% to 10.5%.

Band 7 The $|S|$ results vary a lot but there are only a few good cases, namely NPOESS VIIRS versus Landsat-5 TM, Landsat-4 TM, and EO-1 ALI, as well as Landsat-5 TM versus Landsat-4 TM. For the other sensor comparisons, $|S|$ ranges from 4% to 40%, the worst cases being Terra ASTER with respect to all other sensors ($|S|$ ranging from 25% to 40%).

Please cite this article as: Teillet, P. M. et al. Impacts of spectral band difference effects on radiometric cross-calibration between satellite sensors in the solar-reflective spectral domain. *Remote Sensing of Environment* (2007), doi:10.1016/j.rse.2007.03.003

7.4. Additional comments on results

There are no sensor cross-calibration comparisons for which the entire Landsat solar-reflective spectral domain yields good results if SBDEs are not taken into consideration. Among the four ground target types considered, the RVPN site proved to be the best overall. Except for sensor comparisons involving Terra MISR, RVPN is a good site for the three spectral bands in the visible. SNOW compares favourably with RVPN in the visible and is better than RVPN in the near-infrared. Brown vegetation characteristic of rangeland as represented by the NCRA target (Fig. 2 shows a relatively weak chlorophyll absorption dip in the NCRA reflectance spectrum compared to green vegetation) yields SBDE results similar to those for SAND. SAND is slightly better than NCRA in all spectral regions except the red where NCRA is significantly better and where the comparisons involving MISR are good (MISR is a problem case for the other three ground targets).

For comparisons of Landsat-7 ETM+ and Ikonos, the results presented in this paper are generally consistent with those of Goward et al. (2003), who used a much wider selection of ground targets because their focus was more on product validation than sensor calibration. They found that, on average, Ikonos TOA reflectances in the blue, green, red and NIR bands are lower (4%), higher (3%), higher (3%) and lower (6%), respectively, than Landsat-7 ETM+ TOA reflectances in the analogous spectral bands. The results presented here are in the same directions in the same bands except for a few cases where the *S* results are within 1% and hence explicable by the different selection of ground targets.

8. Spectral characteristics of terrestrial scenes in the Landsat domain

The purpose of this section is to look more closely at scene spectral content to clarify the main factors that give rise to spectral band difference effects. In the context of radiometric cross-calibration between satellite sensors, the sensor responsivity comparison is given by Eqs. (5) and (8), such that

$$\begin{aligned} M_{\mathrm{i}} &= A_{\mathrm{i}}\Delta Q_{\mathrm{iX}}/\Delta Q_{\mathrm{iR}} \\ &= (\Delta Q_{\mathrm{iX}}/\Delta Q_{\mathrm{iR}})\ (\rho_{\mathrm{i}}^{*}E_{0\mathrm{i}}\cos\theta)_{\mathrm{R}}/(\rho_{\mathrm{i}}^{*}E_{0\mathrm{i}}\cos\theta)_{\mathrm{X}}, \end{aligned} \tag{14}$$

where the ΔQ_{i} are the bias-corrected image data. Thus, the spectral dependence enters the cross-calibration in spectral band i via the ratio of $\rho^{*}{}_{\mathrm{i}}\ E_{0\mathrm{i}}$ for the two imaging sensors being compared, where $\rho^{*}{}_{\mathrm{i}}$ is

$$\rho_{\mathrm{i}}^{*} = \textit{Integral over Band } i\{\rho^{*}(\lambda)d(\lambda)\}. \tag{15}$$

Hence, in the formulation used in the CAM5S code,

$$\begin{aligned} \rho_i^{*}E_{0i} = \textit{Integral over Band } i\{&[\rho(\lambda)\tau_S(\lambda)\tau_V(\lambda)\tau_G(\lambda) \\ &+\eta(\lambda)]E_0(\lambda)d(\lambda)\}, \end{aligned} \tag{16}$$

where $\rho(\lambda)$ is the surface spectral reflectance, $\tau_{\mathrm{G}}(\lambda)$ is the atmospheric gas transmittance (O_2, H_2O, O_3, and CO_2), and $\tau_{\mathrm{S}}(\lambda)$ and $\tau_{\mathrm{V}}(\lambda)$ are the scattering transmittances (Rayleigh and aerosol) for the atmospheric paths in the solar illumination and viewing directions, respectively, all as a function of wavelength, λ. The $\eta(\lambda)$ term represents quantities that are second-order and that vary slowly with wavelength (such as atmospheric path radiance).

The integrand in Eq. (16), without the $\eta(\lambda)$ term, is plotted in Fig. 3 for the RVPN and NCRA sites (for US62, AOD55 = 0.05, and SZA = 60°). The uppermost plots in the figure include the full solar-reflective spectral domain pertinent to this study and the subsequent plots show the same data in the spectral regions occupied by the six Landsat spectral bands. By far, most of the high-frequency and low-frequency spectral variability is due to the gas transmittance, $\tau_{\mathrm{G}}(\lambda)$. The main atmospheric gas absorption features are due to: O_3 in spectral band 2; O_2 (0.685 μm) and H_2O (0.72 μm) in spectral band 3; O_2 (0.76 μm) and H_2O (0.825 μm and above 0.9 μm) in spectral band 4; H_2O in spectral band 5; and CO_2 (2.0–2.1 μm), H_2O (2.2 μm) and CH_4 (2.2–2.4 μm) in spectral band 7. These features are modulated by the exo-atmospheric solar irradiance, $E_0(\lambda)$, which contributes to some of the high-frequency and low-frequency spectral variability. For the four ground targets considered here, the surface reflectance, $\rho(\lambda)$, varies more slowly and to a much lesser degree than the aforementioned quantities across any given Landsat spectral band. Finally, as is well known, the two-way scattering transmittance, $\tau_{\mathrm{S}}(\lambda)\ \tau_{\mathrm{V}}(\lambda)$, varies still more slowly across the solar-reflective spectral domain and has no higher-frequency spectral variability at all. Nevertheless, unlike in the other spectral bands, the spectral behaviour in spectral band 1 is not due to gas absorption but rather due to a mix of $E_0(\lambda)$, $\rho(\lambda)$, and the Rayleigh component of $\tau_{\mathrm{S}}(\lambda)$ and $\tau_{\mathrm{V}}(\lambda)$. A visual comparison of Fig. 1 (sensor spectral band response functions) and Fig. 3 readily indicates why spectral band differences arise and why the differences can be significant, as quantified in the results presented in the previous sections.

9. Effects of assumed atmospheric states

The results highlighted so far have been estimates of imaging sensor cross-calibration errors that can arise if spectral band difference effects are not taken into account. In particular, it was noted that atmospheric spectral variability convolved with different sensor spectral response functions is the primary contributor to these errors. However, the simulation results presented so far assumed the same atmospheric state (US62, AOD = 0.05) for all of the sensors considered in order to put all of the comparisons on the same footing. The question arises as to what happens to the SBDEs if the atmospheric state differs from the assumed state. As an initial response to this question, simulation runs were made for different cases, as noted earlier (Table 5): Tropical atmospheric model and AOD55 = 0.5 (for comparisons with respect to results for US62 atmospheric model and AOD55 = 0.05). Results for different solar zenith angles were also compared (SZA = 15° versus 60°), but the differences in SBDE results were negligible in all spectral bands for all ground targets and sensor combinations considered. (The SNOW target was

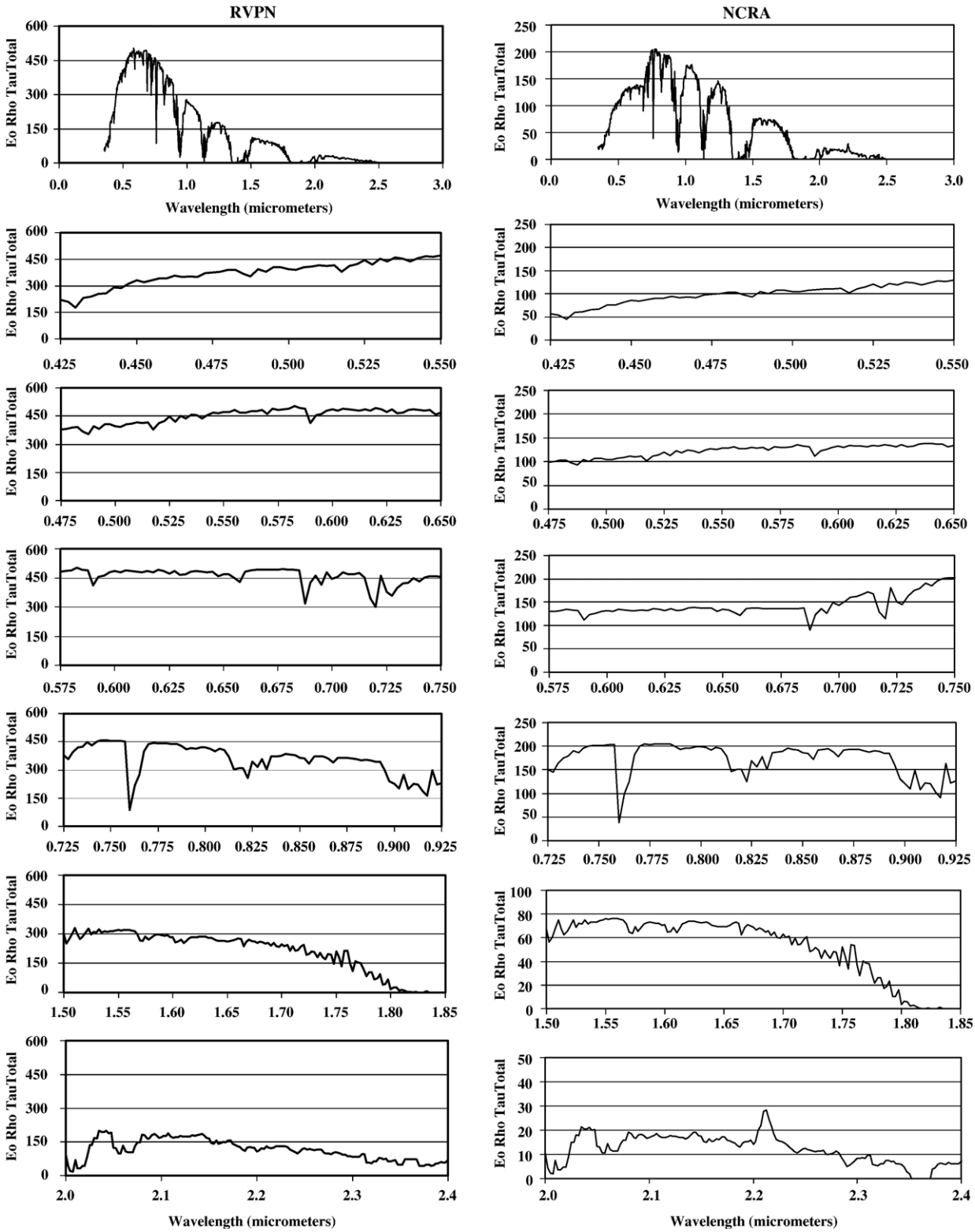

Fig. 3. The key parts of the integrand from Eq. (16) are plotted as a function of wavelength for RVPN (left) and NCRA (right). The uppermost plot on each side shows the full solar-reflective spectral domain pertinent to this study and the subsequent plots show the same data in the spectral regions occupied by the six Landsat spectral bands. Rho = $\rho(\lambda)$ and TauTotal = $\tau_S(\lambda)\ \tau_V(\lambda)\ \tau_G(\lambda)$.

excluded from these comparisons involving the Tropical atmospheric model.) The expectation is that differences in SBDE results for these different atmospheric states should not be strongly dependent on the ground target type or on aerosol optical depth. Moreover, the biggest differences should occur in spectral bands 4 and 5, given the strong spectral variability

ARTICLE IN PRESS

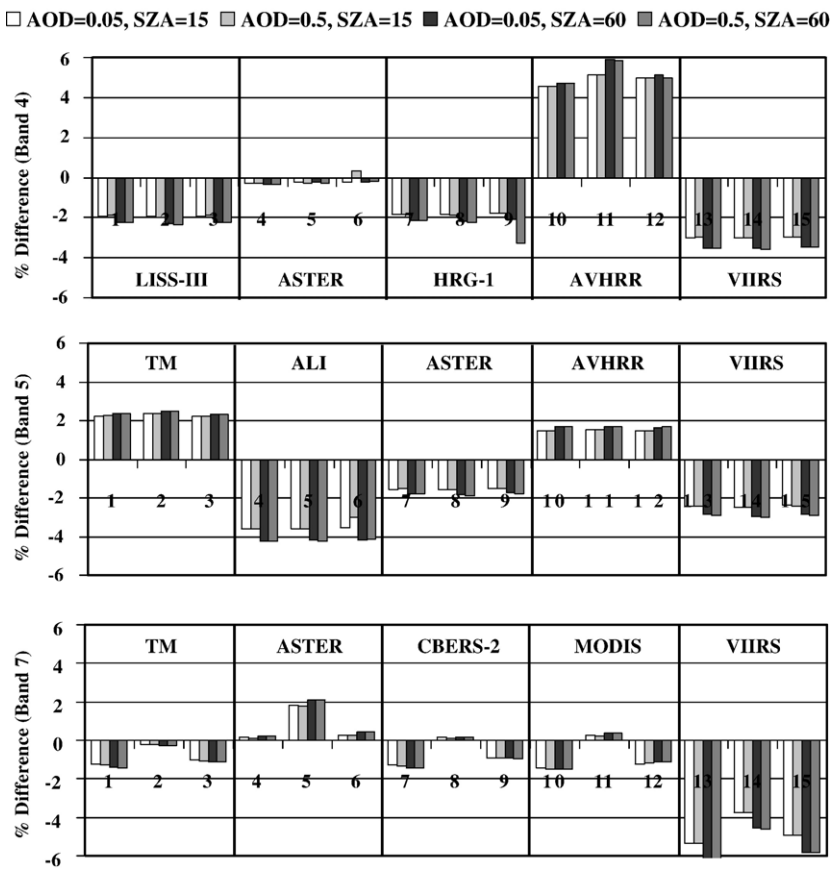

Fig. 4. Examples of percentage differences (100 $(T-U)/U$%) between SBDE factors for US62 (U) and Tropical (T) atmospheric models in analog spectral bands 4, 5 and 7. Results for the different AOD and SZA cases are in the four-bar sets, where the AOD and SZA cases indicated at the top of the figure are at 0.55 μm and in degrees, respectively. The results for sequences of three of the four-bar sets are for, in order, the RVPN, SAND, and NCRA ground targets. The cross-calibration case for each such sequence of three is for the indicated sensor versus Landsat-7 ETM+.

in atmospheric gas transmittance in those spectral regions (Fig. 3).

Percentage differences between SBDE factors, S, for the US62 atmospheric cases, $S(U)$, and the Tropical atmospheric cases, $S(T)$, were defined as

$$D = 100[S(T) - S(U)]/S(U)\% \tag{17}$$

D values were obtained only for cases involving Landsat-7 ETM+ versus other imaging sensors and not for all of the many other possible sensor cross-comparisons. Thus, the following results are limited to these comparisons. Also, the results are intended only to be indicative of the kind of effects that can arise; the full range of potential values for atmospheric parameters under all possible conditions has not been examined. For spectral bands 1–3, the absolute values of D are generally well within 1%. The absolute values of D for spectral band 4 are in the 2% to 5% range and for spectral band 5 in the 2% to 4% range. For spectral band 7, the absolute values of D are generally in the 1% to 2% range, with a notable exception of 4% to 6% for the NPOESS VIIRS versus Landsat-7 ETM+ case. Fig. 4 plots representative examples of D results for spectral bands 4, 5 and 7. The implication of these results is that the use of a standard value for atmospheric water vapour content instead of actual values can, potentially, affect cross-calibrations in these spectral bands by anywhere from less than 1% to as much as 6%. Fig. 4 also indicates that there is negligible dependence on aerosol optical depth and that the dependence on ground target type is generally small, as expected. The ground-target dependence across the three ground target types is worst for sensor comparisons in spectral band 7 and for AVHRR versus ETM+ in spectral band 4.

10. Concluding remarks

Spectral band difference effects (SBDE) have been investigated in the context of radiometric cross-calibration between multiple satellite sensors in the Landsat solar-reflective spectral domain. The simulation study results indicate how large SBDEs can be and for which sensor cross-calibration comparisons they are significant. Moreover, the results presented here clearly show that, except for a limited number of cases, sound cross-calibration requires that the spectral dependencies of the sensor responses and the scene (illumination, atmosphere, and surface) be taken into account. Indeed, even for the Railroad Valley Playa, a target that has relatively low spectral variability across most wavelength regions of interest, one can only ignore SBDEs in selected cases. Thus, lower-cost cross-calibration methodologies that seek to complement the more accurate

Please cite this article as: Teillet, P. M. et al. Impacts of spectral band difference effects on radiometric cross-calibration between satellite sensors in the solar-reflective spectral domain. *Remote Sensing of Environment* (2007), doi:10.1016/j.rse.2007.03.003

calibrations that often (but not always) result from costly field campaigns should somehow take SBDEs into account.

The following spectroradiometric data and tools are recommended to facilitate cross-calibration between satellite sensors.

- On-line repositories of:
  - ➢ Calibration coefficient histories for as many Earth observation sensors as possible.
  - ➢ Relative spectral response profiles for as many Earth observation sensors as possible.
  - ➢ Bi-directional reflectance spectra for the surfaces of key calibration test sites.
  - ➢ Spatial variability and temporal stability indicators for the surfaces of key calibration test sites.
  - ➢ Atmospheric conditions at key calibration test sites.
- Tools for easy transformations between wavelength grids to facilitate comparisons.

Agencies that assume responsibility for one or more of these repositories should coordinate their activities with the Group on Earth Observations (GEO) Secretariat and the Committee on Earth Observation Satellites (CEOS) Working Group on Calibration and Validation (WGCV).

It is strongly recommended that the spectral band difference question receive further examination, not only in the context of sensor calibration but also with respect to impacts on vegetation indices used in vegetation monitoring. Although the SBDE is scene-dependent and, hence, not corrected easily in general, work needs to be done to provide guidance and procedures to the user communities that make use of data from multiple satellite sensors. The goals of the Global Earth Observation System of Systems (GEOSS) initiative will not easily be met if the problem of spectral band differences is not addressed thoroughly.

While it would be advantageous to have satellite sensors with at least a small subset of standardized spectral bands in common (Teillet et al., 1997b), the technical feasibility of such an initiative would have to be addressed. As for the financial feasibility, any additional cost to achieve such standardization would, arguably, be more than recovered by savings in user efforts required to standardize data sets after satellite data acquisition. At the very least, a systematic attempt should be made to ensure that the main optical calibration test sites around the world are fully characterized spectrally with respect to their surface and atmospheric conditions (Ahern et al., 1991; Teillet et al., 2001a,c).

Acknowledgements

The support of the Land Cover Satellite Project Office (NASA Goddard Space Flight Center, Greenbelt, Maryland) for portions of this work is gratefully acknowledged.

References

Ahern, F. J., Gauthier, R. P., Teillet, P. M., Sirois, J., Fedosejevs, G., & Lorente, D. (1991). An Investigation of Continental Aerosols with High Spectral Resolution Solar Extinction Measurements. *Applied Optics*, *30*(36), 5276−5287.

Barnes, R. A., Eplee, R. E., Patt, F. S., & McClain, C. R. (1999). Changes in the radiometric sensitivity of SeaWiFS determined from lunar and solar-based measurements. *Applied Optics*, *38*, 4649−4664.

Black, S. E., Helder, D. L., & Schiller, S. J. (2003). Irradiance-based cross-calibration of Landsat-5 and Landsat-7 Thematic Mapper sensors. *International Journal of Remote Sensing*, *24*(2), 287−304.

Biggar, S. F., Slater, P. N., & Gellman, D. I. (1994). Uncertainties in the in-flight calibration of sensors with reference to measured ground sites in the 0.4 to 1.1 μm range. *Remote Sensing of Environment*, *48*, 245−252.

Biggar, S. F., Thome, K. J., & Wisniewski, W. (2003). Vicarious Radiometric Calibration of EO-1 Sensors by Reference to High-Reflectance Ground Targets. *IEEE Transactions on Geoscience and Remote Sensing*, *41*(6), 1174−1179.

Cabot, F., Hagolle, O., & Henry, P. (2000). Relative and multi-temporal calibration of AVHRR, SeaWiFS, and Vegetation using POLDER characterization of desert sites. *Proceedings of the International Geoscience and Remote Sensing Symposium (IGARSS)*, *Vol. 5* (pp. 2188−2190).

Cabot, F., Hagolle, O., Ruffel, C., & Henry, P. (1999). Use of remote sensing data repository for in-flight calibration of optical sensors over terrestrial targets. *Proceedings of SPIE Conference 3750 on Earth Observing Systems IV, Denver, Colorado* (pp. 514–523).

Chander, G., Helder, D. L., Markham, B. L., Dewald, J. D., Kaita, E., Thome, K. J., et al. (2004). Absolute Landsat-5 TM Reflective-Band Absolute Radiometric Calibration. *IEEE Transactions on Geoscience and Remote Sensing*, *42*(12), 2747−2760.

Chander, G., & Markham, B. (2003). Revised Landsat-5 TM Radiometric Calibration Procedures and Postlaunch Dynamic Ranges. *IEEE Transactions on Geoscience and Remote Sensing*, *41*(11), 2674−2677.

Che, N., Xiong, X., & Barnes, W. (2003). On-Orbit Spectral Characterization Results for Terra MODIS Reflective Solar Bands. *Proceedings of SPIE Conference 5151 on Sensors, Systems, and Next-Generation Satellites, San Diego, California* (pp. 367–374).

Cosnefroy, H., Leroy, M., & Briottet, X. (1996). Selection and characterization of Saharan and Arabian Desert sites for the calibration of optical satellite sensors. *Remote Sensing of Environment*, *58*(1), 101−114.

Dinguirard, M., & Slater, P. N. (1999). Calibration of Space—Multispectral Imaging Sensors: A Review. *Remote Sensing of Environment*, *68*(3), 194−205.

Flittner, D. E., & Slater, P. N. (1991). Stability of Narrow-Band Filter Radiometers in the Solar-Reflective Range. *Photogrammetric Engineering and Remote Sensing*, *57*(2), 165−171.

Godden, G. D., & McKay, C. A. (1997). A Strategy for Observing the Moon to Achieve Precise Radiometric Stability Monitoring. *Canadian Journal of Remote Sensing*, *23*(4), 333−341.

Goward, S. N., Davis, P. E., Fleming, D., Miller, L., & Townshend, J. R. (2003). Empirical comparison of Landsat 7 and IKONOS multispectral measurements for selected Earth Observation System (EOS) validation sites. *Remote Sensing of Environment*, *88*, 80−99.

Gu, X. F., Guyot, G., & Verbrugghe, M. (1992). Evaluation of measurement errors in ground surface reflectance for satellite calibration. *International Journal of Remote Sensing*, *13*(14), 2531−2546.

Helder, D. L., Ruggles, T. A., Dewald, J. D., & Madhavan, S. (2004). Landsat-5 Thematic Mapper Reflective-Band Radiometric Stability. *IEEE Transactions on Geoscience and Remote Sensing*, *42*(12), 2730−2746.

Hill, J., & Aifadopoulou, D. (1990). Comparative analysis of Landsat-5 TM and SPOT HRV-1 data for use in multiple sensor approaches. *Remote Sensing of Environment*, *34*, 55−70.

Iwabuchi, H. (2003). Calibration of the visible and near-infrared channels of NOAA-11 and -14 AVHRRs by using reflections from molecular atmosphere and stratus cloud. *International Journal of Remote Sensing*, *24*(24), 5367−5378.

Kaufman, Y. J., & Holben, B. N. (1993). Calibration of the AVHRR visible and near-IR bands by atmospheric scattering, ocean glint and desert reflection. *International Journal of Remote Sensing*, *14*, 21−52.

Kieffer, H. H., & Wildey, R. L. (1996). Establishing the Moon as a Spectral Radiance Standard. *Journal of Atmospheric and Oceanic Technology*, *13*(2), 360−375.

Koepke, P. (1982). Vicarious satellite calibration in the solar spectral range by means of calculated radiances and its application to Meteosat. *Applied Optics*, *21*(15), 2845−2854.

Loeb, N. G. (1997). In-flight calibration of NOAA AVHRR visible and near-IR bands over Greenland and Antarctica. *International Journal of Remote Sensing*, *18*, 477−490.

Markham, B. L., Boncyk, W. C., Helder, D. L., & Barker, J. L. (1997). Landsat-7 Enhanced Thematic Mapper Plus Radiometric Calibration. *Canadian Journal of Remote Sensing*, *23*(4), 318−332.

Markham, B. L., Thome, K. J., Barsi, J. A., Kaita, E., Helder, D. L., Barker, J. L., et al. (2004). Landsat-7 ETM+ On-Orbit Reflective-Band Radiometric Stability and Absolute Calibration. *IEEE Transactions on Geoscience and Remote Sensing*, *42*(12), 2810−2820.

Martiny, N., Santer, R., & Smolskaia, I. (2005). Vicarious calibration of MERIS over dark waters in the near infrared. *Remote Sensing of Environment*, *94* (4), 475−490.

Nieke, J., Aoki, T., Tanikawa, T., Motoyoshi, H., Hori, M., & Nakajima, Y. (2003). Cross-calibration of satellite sensors over snow fields. In W. L. Barnes (Ed.), *Proceedings of SPIE Conference 5151 on Earth Observing Systems VIII, SPIE*, *Vol. 5151* (pp. 406−414). San Diego, California.

O'Brien, D. M., & Mitchell, R. M. (2001). An Error Budget for Cross-Calibration of AVHRR Shortwave Channels against ATSR-2. *Remote Sensing of Environment*, *75*, 216−229.

O'Brien, H. W., & Munis, R. H. (1975). *Red and Near-Infrared Spectral Reflectance of Snow.CRREL Research Report*, *Vol. 332*. Hanover, New Hampshire Cold Regions Research and Engineering Laboratory 18 pages.

O'Neill, N. T., Royer, A., & Nguyen, M. N. (1996). *Scientific and Technical Report on the Development of a Modified Version of the H5S Code which Incorporates Major Features of the 6S Code.* CARTEL Internal Report CARTEL-1996-020, CARTEL, Department de géographie et télédétection, 2500, boul. de l'Université, Université de Sherbrooke, Sherbrooke, Québec, Canada J1K 2R1 62 pp.

Rao, C. R. N., Cao, C., & Zhang, N. (2003). Inter-calibration of the Moderate-Resolution Imaging Spectroradiometer and the Along-Track Scanning Radiometer-2. *International Journal of Remote Sensing*, *24*(9), 1913−1924.

Rao, C. R. N., & Chen, J. (1995). Inter-satellite calibration linkages for the visible and near-infrared channels of the Advanced Very High Resolution Radiometer on the NOAA-7,-9, and -11 spacecraft. *International Journal of Remote Sensing*, *16*, 1931−1942.

Rao, C. R. N., & Chen, J. (1999). Revised post-launch calibration of the visible and near-infrared channels of the Advanced Very High Resolution Radiometer (AVHRR) on the NOAA-14 spacecraft. *International Journal of Remote Sensing*, *20*, 3485−3491.

Rondeaux, G., Steven, M. D., Clark, J. A., & Mackay, G. (1998). La Crau: A European test site for remote sensing validation. *International Journal of Remote Sensing*, *19*, 2775−2788.

Santer, R., Gu, X. F., Guyot, G., Deuzé, J. L., Devaux, C., Vermote, E., et al. (1992). SPOT calibration at the La Crau test site (France). *Remote Sensing of Environment*, *41*(2–3), 227−237.

Santer, R., & Martiny, N. (2003). Sky radiance measurements for ocean colour calibration-validation. *Applied Optics*, *42*(6), 896−907.

Schiller, S. J. (2003). Technique for estimating uncertainties in top-of-atmosphere radiances derived by vicarious calibration. In W. L. Barnes (Ed.), *Proceedings of SPIE Conference 5151 on Earth Observing Systems VIII, SPIE*, *Vol. 5151* (pp. 502−516). San Diego, California.

Six, D., Fily, M., Alvain, S., Henry, P., & Benoist, J. -P. (2004). Surface Characterisation of the Dome Concordia Area (Antarctica) as a Potential Satellite Calibration Site, Using SPOT 4/VEGETATION Instrument. *Remote Sensing of Environment*, *89*, 83−94.

Slater, P. N., Biggar, S. F., Holm, R. A., Jackson, R. D., Mao, Y., Moran, M. S., et al. (1987). Reflectance- and Radiance-Based Methods for In-Flight Absolute Calibration of Multispectral Sensors. *Remote Sensing of Environment*, *22*, 11−37.

Slater, P. N., Biggar, S. F., Palmer, J. M., & Thome, K. J. (2001). Unified Approach to Absolute Radiometric Calibration in the Solar-Reflective Range. *Remote Sensing of Environment*, *77*, 293−303.

Staetter, R., & Schroeder, M. (1978). Spectral characteristics of natural surfaces. *Proceedings of the Tenth International Conference on Earth Observations from Space, ESA-SP 134*.

Steven, M. D., Malthus, T. J., Baret, F., Xu, H., & Chopping, M. J. (2003). Intercalibration of vegetation indices from different sensor systems. *Remote Sensing of Environment*, *88*, 412−422.

Suits, G. H., Malila, W. A., & Weller, T. M. (1988). The Prospects for Detecting Spectral Shifts Due to Satellite Sensor Ageing. *Remote Sensing of Environment*, *26*, 17−29.

Tahnk, W. R., & Coakley, J. A. (2001). Updated calibration coefficients for NOAA-14 AVHRR channels 1 and 2. *International Journal of Remote Sensing*, *22*(15), 3053−3057.

Tanré, D., Deroo, C., Duhaut, P., Herman, M., Morcrette, J. J., Perbos, J., et al. (1990). Description of a computer code to simulate the satellite signal in the solar spectrum: the 5S code. *International Journal of Remote Sensing*, *11* (4), 659−668.

Teillet, P. M. (1990). Effects of Spectral Shifts on Sensor Response. *Proceedings of the ISPRS Commission VII Symposium(pp. 59–65). Victoria, B.C.*

Teillet, P. M. (1997). A Status Overview of Earth Observation Calibration/Validation for Terrestrial Applications. *Canadian Journal of Remote Sensing*, *23*(4), 291−298.

Teillet, P. M., Fedosejevs, G., & Gauthier, R. P. (1998). Operational Radiometric Calibration of Broadscale Satellite Sensors Using Hyperspectral Airborne Remote Sensing of Prairie Rangeland: First Trials. *Metrologia*, *35*, 639−641.

Teillet, P. M., Thome, K. J., Fox, N., & Morisette, J. T. (2001a). Earth Observation Sensor Calibration Using A Global Instrumented and Automated Network of Test Sites (GIANTS). In H. Fujisada, J. B. Lurie, & K. Weber (Eds.), *Proceedings of SPIE Conference 4550 on Sensors, Systems, and Next-Generation Satellites V, SPIE*, *Vol. 4550* (pp. 246−254). Toulouse, France.

Teillet, P. M., Barker, J. L., Markham, B. L., Irish, R. R., Fedosejevs, G., & Storey, J. C. (2001b). Radiometric cross-calibration of the Landsat-7 ETM+ and Landsat-5 TM sensors based on tandem data sets. *Remote Sensing of Environment*, *78*, 39−54.

Teillet, P. M., Fedosejevs, G., Gauthier, R. P., O'Neill, N. T., Thome, K. J., Biggar, S. F., et al. (2001c). A Generalized Approach to the Vicarious Calibration of Multiple Earth Observation Sensors Using Hyperspectral Data. *Remote Sensing of Environment*, *77*(3), 304−327.

Teillet, P. M., Fedosejevs, G., Gauthier, R. P., Shin, R. T., O'Neill, N. T., Thome, K. J., et al. (1999). Radiometric calibration of multiple Earth observation sensors using airborne hyperspectral data at the Newell County rangeland test site. *Proceedings of the SPIE Conference on Earth Observing Systems IV, SPIE*, *Vol. 3750* (pp. 470−481). Denver, Colorado.

Teillet, P. M., Helder, D. L., Ruggles, T. A., Landry, R., Ahern, F. J., Higgs, N. J., et al. (2004). A Definitive Calibration Record for the Landsat-5 Thematic Mapper Anchored to the Landsat-7 Radiometric Scale. *Canadian Journal of Remote Sensing*, *30*(4), 631−643.

Teillet, P. M., Horler, D. N. H., & O'Neill, N. T. (1997a). Calibration/Validation, Stability Monitoring, and Quality Assurance in Remote Sensing: A New Paradigm. *Canadian Journal of Remote Sensing*, *23*(4), 401−414.

Teillet, P. M., Markham, B. L., & Irish, R. R. (2006). Landsat cross-calibration based on near simultaneous imaging of common ground targets. *Remote Sensing of Environment*, *102*(3–4), 264−270.

Teillet, P. M., & Santer, R. P. (1991). Terrain Elevation and Sensor Altitude Dependence in a Semi-Analytical Atmospheric Code. *Canadian Journal of Remote Sensing*, *17*(1), 36−44.

Teillet, P. M., Slater, P. N., Ding, Y., Santer, R. P., Jackson, R. D., & Moran, M. S. (1990). Three Methods for the Absolute Calibration of the NOAA AVHRR Sensors In-Flight. *Remote Sensing of Environment*, *31*, 105−120.

Teillet, P. M., Staenz, K., & Williams, D. J. (1997b). Effects of Spectral, Spatial, and Radiometric Characteristics on Remote Sensing Vegetation Indices for Forested Regions. *Remote Sensing of Environment*, *61*, 139−149.

Thome, K. J. (2001). Absolute Radiometric Calibration of Landsat 7 ETM+ Using the Reflectance-Based Method. *Remote Sensing of Environment*, *78* (1–2), 27−38.

Thome, K. J., Crowther, B. G., & Biggar, S. F. (1997). Reflectance- and Irradiance-Based Calibration of Landsat-5 Thematic Mapper. *Canadian Journal of Remote Sensing*, *23*, 309−317.

Thome, K. J., Biggar, S. F., & Wisniewski, W. (2003a). Cross Comparison of EO-1 Sensors and Other Earth Resources Sensors to Landsat-7 ETM+ Using Railroad Valley Playa. *IEEE Transactions on Geoscience and Remote Sensing*, *41*, 1180−1188.

Please cite this article as: Teillet, P. M. et al. Impacts of spectral band difference effects on radiometric cross-calibration between satellite sensors in the solar-reflective spectral domain. *Remote Sensing of Environment* (2007), doi:10.1016/j.rse.2007.03.003

ARTICLE IN PRESS

Thome, K. J., Czapla-Myers, J., & Biggar, S. (2003b). Vicarious calibration of Aqua and Terra MODIS. In W. L. Barnes (Ed.), *Proceedings of SPIE Conference 5151 on Earth Observing Systems VIII, SPIE*, *Vol. 5151* (pp. 395−405). San Diego, California.

Thome, K., Schiller, S., Conel, J., Arai, K., & Tsuchida, S. (1998). Results of the 1996 Earth Observing System vicarious calibration joint campaign at Lunar Lake Playa. *Metrologia*, *35*, 631−638.

Trishchenko, A. P., Cihlar, J., & Li, Z. (2002). Effects of Spectral Response Function on Surface Reflectance and NDVI Measured with Moderate Resolution Satellite Sensors. *Remote Sensing of Environment*, *81*(1), 1−18.

Vermote, E. F., & Kaufman, Y. J. (1998). Absolute Calibration of AVHRR Visible and Near-Infrared Channels Using Ocean and Cloud Views. *International Journal of Remote Sensing*, *16*(13), 2317−2340.

Vermote, E., Tanré, D., Deuzé, J. L., Herman, M., & Morcette, J. J. (1997). Second simulation of the satellite signal in the solar spectrum: an overview. *IEEE Transactions on Geoscience and Remote Sensing*, *35*(3), 675−686.

Wheeler, R. J., LeCroy, S. R., Whitlock, C. H., Purgold, G. C., & Swanson, J. S. (1994). Surface characteristics for the alkali flats and dune regions at White Sands Missile Range, New Mexico. *Remote Sensing of Environment*, *48*, 181−190.

Wu, D., Yin, Y., Wang, Z., Gu, X., Verbrugghe, M., & Guyot, G. (1997). Radiometric characterisation of Dunhuang satellite calibration test site (China). In G. Guyot & T. Phulpin (Eds.), *Physical Measurements and Signatures in Remote Sensing*, *Vol. 1* (pp. 151−160). Rotterdam Balkema.

Please cite this article as: Teillet, P. M. et al. Impacts of spectral band difference effects on radiometric cross-calibration between satellite sensors in the solar-reflective spectral domain. *Remote Sensing of Environment* (2007), doi:10.1016/j.rse.2007.03.003